Macromolecules

Article

pubs.acs.org/Macromolecules

# Effect of Confinement on Proton Transport Mechanisms in Block Copolymer/Ionic Liquid Membranes

Megan L. Hoarfrost,*[,†,‡] Madhu S. Tyagi,[§,∥] Rachel A. Segalman,[†,⊥] and Jeffrey A. Reimer[†,‡]

[†]Department of Chemical and Biomolecular Engineering, University of California, Berkeley, Berkeley, California 94720, United States

[‡]Energy and Environmental Technologies Division and [⊥]Materials Sciences Division, Lawrence Berkeley National Laboratory, Berkeley, California 94720, United States

[§]NIST Center for Neutron Research, Gaithersburg, Maryland 20899, United States

[∥]Department of Materials Science and Engineering, University of Maryland, College Park, Maryland 20742, United States

Supporting Information

**ABSTRACT:** Nanostructured membranes containing structural and proton-conducting domains are of great interest for a wide range of applications requiring high conductivity coupled to high thermal stability. Understanding the effect of nanodomain confinement on proton-conducting properties in such materials is essential for designing new, improved membranes. This relationship has been investigated for a lamellae-forming mixture of poly(styrene-*b*-2-vinyl pyridine) (PS-*b*-P2VP) with ionic liquid composed of imidazole and bis(trifluoromethylsulfonyl)-imide, where the ionic liquid selectively resides in the P2VP domains of the block copolymer. Quasi-elastic neutron scattering and NMR diffusion measurements reveal increased prevalence of a fast proton hopping transport mechanism, which we hypothesize is due to changes in the hydrogen bond structure of the ionic liquid under confinement. This, in combination with unique ion aggregation behavior, leads to a lower activation energy for macroscopic ion transport compared with that in a mixture of ionic liquid with P2VP homopolymer. The proton transference number in both samples is significantly higher than that in the neat ionic liquid, which could be taken advantage of for applications such as proton exchange membrane fuel cells and actuators. These results portend the rational design of nanostructured membranes having improved mechanical properties and conductivity.

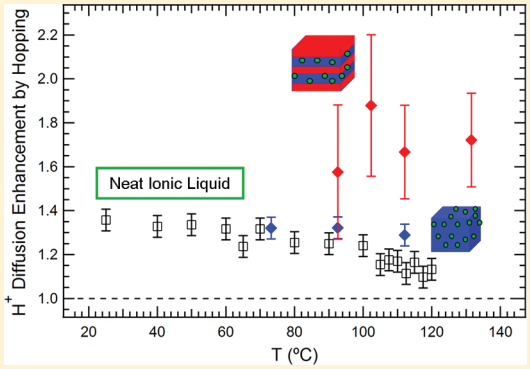


## INTRODUCTION

Nanostructured membranes containing structural and ion-conducting phases are of great interest for a wide variety of applications requiring high ionic conductivity coupled to mechanical durability. Such membranes may be designed to exhibit continuous ion-conducting channels that lead to enhanced conductivity compared with nonordered materials. For instance, Nafion (Dupont) is currently the industry standard proton-conducting polymer membrane for many applications because of its exceptional conductivity and mechanical properties that have been attributed to its nanoscale phase separation into conducting, water-filled domains and structural, hydrophobic domains.[1] Furthermore, materials designed to have well-ordered, continuous nanostructures have significantly higher conductivities than comparable nonordered materials.[2,3] Understanding the effect of morphology on conductivity has become increasingly important in recent years as a tool for designing new, improved membranes.[4−9]

Of the many factors contributing to improved conductivity in nanostructured membranes (including conducting phase continuity and increased contrast between conducting and structural phases[4,8,9]), we expect differences in the local charge carrier environment near the "walls" of conducting phases to have a significant impact on the mechanism of conductivity. It has been shown, for example, that hydrogen bonding is significantly different at the walls of confined water domains[10−13] and that such effects have significant implications for proton transport in hydrated Nafion.[14−18] A few studies of nanostructured materials with ion carriers other than water have also identified wall effects on the mechanism of conductivity.[19,20] These effects were deduced largely based on bulk conductivity measurements. In one case, NMR experiments also provided clues as to how the local dynamics change,[20] but determining exactly how confinement affects the molecular mechanisms of conductivity remains difficult.

Mixing a block copolymer with an ionic liquid is one route to obtaining nanostructured, ion-conducting membranes having high ionic conductivity coupled to favorable mechanical durability. Ionic liquids have been selectively incorporated

Received: December 19, 2011
Revised: March 13, 2012
Published: March 23, 2012

 © 2012 American Chemical Society 

into one phase of a diblock copolymer, where the second phase imparts mechanical durability to the membrane.[21−26] Such membranes self-assemble into well-defined nanostructures, making them ideal materials for studying the relationship between structure and conductivity. In this work, the effect of confinement on the mechanism of conductivity has been investigated for mixtures of the diblock copolymer poly(styrene-*b*-2-vinyl pyridine) (PS-*b*-P2VP) with the proton-conducting ionic liquid, imidazolium:bis(trifluoromethylsulfonyl)imide ([Im][TFSI]) having an excess of imidazole, in which the ionic liquid is selective for the P2VP phase of the block copolymer.

Nonstoichiometric [Im][TFSI] containing excess imidazole conducts protons via two mechanisms: a vehicle mechanism whereby protons are carried by imidazolium cations and a proton-hopping mechanism whereby protons are transferred between hydrogen bonded imidazole molecules.[27] Excess imidazole molecules act as proton "acceptors" that facilitate proton hopping, increasing proton conduction vis-à-vis conduction by vehicle diffusion alone.[28,29] Because the proton-hopping mechanism is strongly related to the hydrogen bond network of imidazole and hydrogen bonding is known to be affected by confinement, we surmise that proton hopping in imidazole will also be affected by confinement (i.e., to block copolymer nanodomains).

Previous studies of block copolymer/ionic liquid membranes have focused on bulk conductivity measurements.[7,21,26,30,31] These measurements have provided insight into the relationship between structure and conductivity but afford limited information regarding the mechanism of ionic liquid conductivity. Combined conductivity and NMR studies of mixtures of ionic liquids with homopolymers and random copolymers have shown that specific interactions between the ionic liquid and polymers greatly affect the prevalence of ion aggregation and the number of effective charge carriers,[32,33] yet there have been no similar studies on mixtures containing protic ionic liquids or having well-defined nanostructures. In this work, we employ a combination of experimental techniques that together probe the dynamics of a variety of molecular and atomic species on length scales ranging from tenths of nanometers to micrometers to millimeters to determine the effect of confinement on the mechanisms of proton transport in a self-assembled mixture of PS-*b*-P2VP block copolymer with nonstoichiometric [Im][TFSI] ionic liquid, where the ionic liquid is confined to P2VP domains. A mixture of nonstoichiometric [Im][TFSI] with P2VP homopolymer has been studied in addition to the block copolymer mixture to discriminate effects of confinement from effects of mixing with P2VP. We show that combining the ionic liquid with both P2VP and PS-*b*-P2VP has significant effects on ion aggregation and the proton transference number and, most strikingly, that the amount of proton hopping compared with vehicle diffusion is greatly increased in the nanostructured membrane. These results portend the rational design of nanostructured membranes having improved mechanical properties and conductivity.

## EXPERIMENTAL SECTION

**Polymer Synthesis and Characterization.** Hydrogenated and deuterated poly(2-vinyl pyridine) (P2VP and *d*P2VP) and poly(styrene-*b*-2-vinyl pyridine) (PS-*b*-P2VP and *d*PS-*b*-*d*P2VP) were synthesized via anionic polymerization as previously described.[34] $d_8$-Styrene monomer (Polymer Source) and $d_7$-2-vinyl pyridine monomer (Isotec) were used to synthesize deuterated polymers. The molecular weights of the polystyrene blocks (PS or *d*PS) were determined using gel permeation chromatography (GPC), and the total molecular weights of the block copolymers were determined using $^1$H NMR (Bruker AVB 300 MHz). The molecular weight of P2VP was determined using $^1$H NMR end-group analysis, and the molecular weight of *d*P2VP was determined using GPC. GPC was used to assess the polydispersity of each polymer. The degree of polymerization of the P2VP or *d*P2VP block, $N_{P2VP}$, the volume fraction of PS or *d*PS, $f_{PS}$, and the polydispersity index (PDI) of each polymer are given in Table 1.

**Table 1. Degree of Polymerization, Volume Fraction, and PDI of Polymers Studied**

| polymer | $N_{P2VP}$ | $f_{PS}$ | PDI |
|---|---|---|---|
| *d*P2VP | 82 | 0.00 | 1.07 |
| *d*PS-*b*-P2VP | 72 | 0.71 | 1.04 |
| P2VP | 118 | 0.00 | 1.07 |
| PS-*b*-P2VP | 101 | 0.72 | 1.04 |

**Ionic Liquid Purification and Preparation.** Imidazole (≥95%), $d_4$-imidazole (≥98% deuteration), and bis(trifluoromethylsulfonyl)-imide (HTFSI, ≥95%) were purchased from Sigma Aldrich and purified by sublimation under vacuum. The final purity of each starting material was assessed using differential scanning calorimetry (DSC) and $^1$H NMR. Purified imidazole or $d_4$-imidazole and HTFSI were combined in a 4:1 molar ratio and heated to 100 °C for 2 to 3 h. The compositions of the resulting nonstoichiometric [Im][TFSI] and [*d*Im][TFSI] ionic liquids were confirmed by comparing the measured melting points and $^1$H NMR profiles to literature.[28] The structures of the ionic liquid molecules are shown in Figure 1. Because of their hygroscopic nature, the ionic liquids and their starting materials were handled in an argon atmosphere glovebox and sealed sample holders at all times.

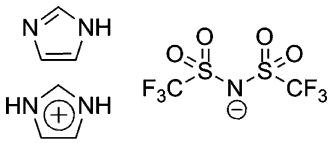

**Figure 1.** Chemical structure of nonstoichiometric [Im][TFSI] molecules.

**Preparation of Polymer/Ionic Liquid Mixtures.** Dichloromethane and tetrahydrofuran were degassed using three freeze, pump, thaw cycles, dried by stirring over $CaH_2$ overnight, and stored on molecular sieves in an argon atmosphere glovebox. All further sample preparation was performed within the glovebox. Predetermined masses of ionic liquids and polymers were added to glass vials. Ca. 5 wt % solutions were prepared by dissolving in dichloromethane (block copolymer mixtures) or tetrahydrofuran (homopolymer mixtures), and the solutions were stirred overnight. Samples were cast one drop at a time into sample holders for DSC, small-angle X-ray scattering (SAXS), quasi-elastic neutron scattering (QENS), and AC impedance spectroscopy. Samples were cast onto pieces of Kapton for NMR. Solvent was removed carefully so as not to remove simultaneously excess imidazole. Block copolymer samples were heated to 65 °C for precisely 30 min. Homopolymer samples were dried at 35 °C for 3 days. Complete solvent removal and negligible imidazole loss were confirmed by $^1$H NMR. After solvent removal, DSC, SAXS, QENS, and conductivity sample holders were sealed shut, whereas NMR samples were scraped off of the Kapton and into sealable NMR tubes (for diffusion measurements) or 4 mm (outer diameter) magic-angle spinning (MAS) rotors. Samples were sealed in jars containing desiccant for transportation to experimental apparatuses. The exclusion of water from samples was confirmed by $^1$H NMR.


dx.doi.org/10.1021/ma202741g | *Macromolecules* 2012, 45, 3112−3120

Both homopolymer and block copolymer samples were prepared and studied to distinguish the effects of mixing the ionic liquid with P2VP from the effects of confining the ionic liquid to nanodomains. The ratio of imidazole molecules to 2VP monomer units was held constant at 1.16:1 for all samples, which translates into 30 mass percent ionic liquid in the block copolymer samples and 59 mass percent ionic liquid in the homopolymer samples. This ensured that the glass-transition temperature of the P2VP/ionic liquid phase, $T_{g,P2VP}$, was constant at ~4 °C for each sample. The specific ionic liquid loading was chosen to maximize the number of ionic liquid protons so as to maximize the signal-to-noise ratio in NMR and QENS experiments while limiting the ionic liquid concentration to the range in which the block copolymer mixtures form lamellar nanostructures. Deuterated polymers were used for NMR experiments so that the ionic liquid protons could be easily resolved in NMR spectra. Deuterated polymers as well as deuterated imidazole were used for QENS experiments so that the dynamics studied were dominated by the acidic proton. Hydrogenated materials were used for AC impedance ionic conductivity measurements.

**Differential Scanning Calorimetry.** DSC samples were crimped in an argon atmosphere glovebox using hermetically sealed pans and placed inside a container with desiccant for transfer to the DSC. DSC was performed on a TA Instruments DSC Q20. Indium and dodecane were used as calibration standards. Samples underwent three heating and cooling cycles with a scan rate of 10 °C/min, and thermal transition temperatures from the second heating scan were recorded.

**Morphology Characterization.** Mixture morphologies were determined using SAXS. Samples of ca. 1 mm thickness were cast in an argon atmosphere glovebox into sample cells formed by an aluminum spacer sealed onto a Kapton window on one side. After heating to remove solvent, a second Kapton window was glued to seal the sample cells, and the cells were sealed in jars containing desiccant for transportation to the beamline. SAXS was performed on beamline 7.3.3 of the Advanced Light Source (ALS) and beamline 1−4 of the Stanford Synchrotron Radiation Lightsource (SSRL). Samples were equilibrated within the beamline at 145 °C for 30−45 min before data were gathered. At the ALS, the X-ray beam was focused to a 50 by 300 $\mu$m spot, and the X-ray wavelength was $\lambda$ = 1.240 Å. Full 2-D scattering patterns were collected on an ADSC CCD detector with an active area of 188 by 188 mm. The scattering patterns were radially averaged, and the scattering intensity was corrected with the postion chamber intensity using Nika version 1.18. At the SSRL, the X-ray beam was focused to a 0.5 mm diameter spot, and the X-ray wavelength was $\lambda$ = 1.488 Å. A single quadrant of a 2-D scattering pattern was collected on a CCD detector with an active area of 25.4 by 25.4 mm. The scattering patterns were radially averaged and corrected for detector null signal, dark current, and empty cell scattering.

The block copolymer mixtures in this study have lamellar morphologies. Scattering patterns are shown in Figures S1a and S1b in the Supporting Information. The deuterated mixture used for NMR and QENS experiments has a lamellar domain size, $d$, of 37 nm, calculated as $2\pi/q^*$, where $q^*$ is the primary scattering peak from SAXS data. The size of the $d$P2VP/ionic liquid channel, then, is 17 nm, assuming complete segregation of the ionic liquid to the $d$P2VP domains, ideal mixing, and the density of the ionic liquid to be 1.4 g/mL (based on volumetric measurements). The assumption of complete ionic liquid segregation is justified based on the strong selectivity of the ionic liquid for P2VP. The strong selectivity of stoichiometric [Im][TFSI] has been previously demonstrated based on the scaling behavior of $d$ with mixture composition.[25] Non-stoichiometric [Im][TFSI] is also very selective for P2VP, as evidenced by an increase in $d$ with increased ionic liquid composition (see Figure S1c in the Supporting Information) as well as negligible change in the glass-transition temperature of the PS phase upon ionic liquid addition. The hydrogenated PS-*b*-P2VP block copolymer used for bulk ionic conductivity measurements has a slightly larger molecular weight than the deuterated version, leading to a larger lamellar domain size of the PS-*b*-P2VP/ionic liquid mixture of $d$ = 43 nm (P2VP/ionic liquid channel size equal to 19 nm).

**Ionic Conductivity Measurements.** Bulk ionic conductivity was measured using four-point probe AC impedance spectroscopy. Samples were cast in an argon atmosphere glovebox into a homemade, airtight, poly(ether ether ketone) cell equipped with rubber o-rings and four stainless-steel electrodes. The working and reference electrodes were 1.7 cm long and placed 0.6 to 0.7 cm apart, and the samples were cast to be ~0.05 cm thick (measured after AC impedance measurements). After solvent removal, the sample cell was screwed shut, removed from the glovebox, and heated to 150 °C for 12 h before measurements were made. AC impedance measurements were performed using a Gamry Reference 600 potentiostat at descending temperatures. An alternating current signal with an amplitude of 5 mV was applied in the frequency range of 0.1 to 65 000 Hz. The nonzero $x$ intercept in the Nyquist plot of the negative imaginary part of the impedance versus the real part of the impedance was taken as the sample resistance, $R$. The ionic conductivity, $\sigma$, was calculated as $t/AR$, where $t$ and $A$ are the thickness and area of the sample (with respect to electrode placement), respectively, measured after the AC impedance measurements.

**Diffusion Coefficient Measurements.** Self-diffusion coefficients were measured with pulsed-field gradient spin echo (PGSE) and pulsed-field gradient stimulated echo (PGStE) NMR experiments using a Doty Scientific single-axis diffusion probe with temperature control. The applied gradients were calibrated using water[35] and glycerol[36] standards and were found to reach 1.7 T/m. $^1$H diffusion coefficients were measured in a 7 T superconducting magnet with a 300 MHz Tecmag Apollo spectrometer and gradient control, and $^{19}$F diffusion coefficients were measured in a 1.5 T superconducting magnet with a 61.2 MHz Tecmag LapNMR spectrometer and gradient control. Experiments were performed between 25 and 132 °C, where the temperature was calibrated[37] using an ethylene glycol standard between 24 and 83 °C and extrapolation to higher temperatures.

The NMR signal attenuation for Fickian diffusion in both PGSE and PGStE experiments is described by

$$I = I_0 \exp( - D\gamma^2 g^2 \delta^2 (\Delta - \delta/3)) \quad (1)$$

where $I$ is the spin−echo signal intensity, $I_0$ is the signal intensity with zero gradient, $\gamma$ is the magnetogyric ratio of the probe nucleus, $g$ is the magnitude of the gradient pulse, $\delta$ is the duration of the gradient pulse, $\Delta$ is the duration of time between the leading edges of the two gradient pulses, and $D$ is the self-diffusion coefficient of the probe nucleus. $I$ was measured as a function of g, and eq 1 was used to determine $D$. Example plots of $I/I_0$ as a function of $\gamma^2 g^2 \delta^2 (\Delta - \delta/3)$ are shown in Figure S2 in the Supporting Information. Experiments were repeated on the block copolymer sample using values of $\Delta$ ranging from 0.02 to 0.11 s, corresponding to root-mean-squared diffusion path lengths of ionic liquid ions ranging from 0.2 to 2.2 $\mu$m, resulting in consistent measurements of $D$. (See, for example, Figure S3 in the Supporting Information.) PGSE and PGStE experiments performed on each sample also resulted in consistent measurements of $D$.

Spectroscopic resolution of ionic liquid protons was possible in $^1$H experiments because the polymers were deuterated. Thus, the diffusion coefficients for protons covalently bound to the carbon atoms on the imidazole (involved only in vehicle diffusion), $D_{C-H}$, and protons bound to nitrogen atoms on imidazole (involved in vehicle diffusion and proton hopping), $D_{N-H}$, were measured separately. For $^{19}$F experiments, a single peak was observed corresponding to fluorine atoms on the TFSI anion, and a single diffusion coefficient measured, $D_{TFSI}$.

**Magic-Angle Spinning NMR.** High-resolution $^1$H NMR spectra were obtained for ionic liquid/polymer mixtures using MAS NMR. MAS experiments were performed in a 7 T superconducting magnet using a Doty Scientific MAS probe and 300 MHz Tecmag Apollo spectrometer. Samples were annealed in sealed 4 mm (outer diameter) MAS rotors at 150 °C for 12 h before MAS experiments. During MAS experiments, samples were spun at 13 kHz. Spectra were acquired between 93 and 132 °C, where the temperature was calibrated in the same manner as they were for diffusion measurements. Samples equilibrated slowly at each temperature due to fast spinning, so

samples were annealed at each temperature for 1−9 h until the spectra did not change between consecutive acquisitions.

**Quasi-Elastic Neutron Scattering.** QENS experiments were performed at the National Institute for Standards and Technology (NIST) Center for Neutron Research (NCNR) on the high flux backscattering spectrometer (HFBS). An incident neutron wavelength of $\lambda$ = 6.271 Å and an energy resolution of ~0.8 $\mu$eV were used. Data from all 16 detectors were used to probe a $q$ range from 0.25 to 1.75 Å$^{-1}$. Polymer/ionic liquid samples were loaded into sample cans with an annular geometry, and the sample transmission was set to ~90% to minimize multiple scattering. All experiments were performed at 140 °C. The acquired data were corrected for detector efficiencies (determined using a vanadium standard), and the resolution function of the instrument was determined by measuring scattering from the *d*P2VP/[*d*Im][TFSI] mixture at 15 K where all of the signal is expected to be elastic.

Elastic and quasi-elastic scattering contribute to the observed scattering profiles, $S(q,\omega)$. Quasi-elastic scattering in $S(q,\omega)$ reflects self-correlated motion and appears as broad signal over a sharp, elastic scattering peak centered around $\omega$ = 0. Reduction, visualization, and analysis of HFBS data were performed using the DAVE software package developed at NCNR.[38] The elastic scattering contributions were modeled using a Delta function convoluted with the resolution function of the instrument. The quasi-elastic scattering contributions were modeled using two Lorentzian functions, one for the high-energy background signal and one for the main quasi-elastic contribution in the energy range of the instruments. The full width at half-maximum (fwhm) values of the high-energy background signals were found to be essentially constant at 30 $\mu$eV for all $q$. Fitted fwhm's of the main quasi-elastic contributions in HFBS profiles were reported, with the standard deviation of the fits reported as the error.

## RESULTS AND DISCUSSION

Relative cation and anion diffusion in nonstoichiometric [Im][TFSI] was found to be dramatically affected both by combining the ionic liquid with polymer as well as confining it to lamellar block copolymer nanodomains. Whereas the anion and cation diffuse at similar rates in the neat ionic liquid,[28,39] the cation diffuses much more quickly than the anion when the ionic liquid is added to the homopolymer or block copolymer, as shown in Figure 2. Faster cation diffusion can be attributed to the prevalence of anionic aggregates in the membrane or to specific interactions between the TFSI anions and the 2VP repeat units. The presence of anionic aggregates has been shown to cause relatively fast cation diffusion in ionic liquid-impregnated Nafion at low hydration levels.[32] Alternatively, specific polymer/anion interactions may slow anion diffusion. This effect has been previously observed in mixtures of 1-ethyl-3-methylimidazolium/TFSI with poly(methyl methacrylate) (PMMA).[33] The 2VP repeat unit is basic, so this type of specific interaction with TFSI is not anticipated. It is possible, however, that some 2VP moieties are protonated by imidazolium, leading to interactions between protonated 2VP moieties and the TFSI anion.

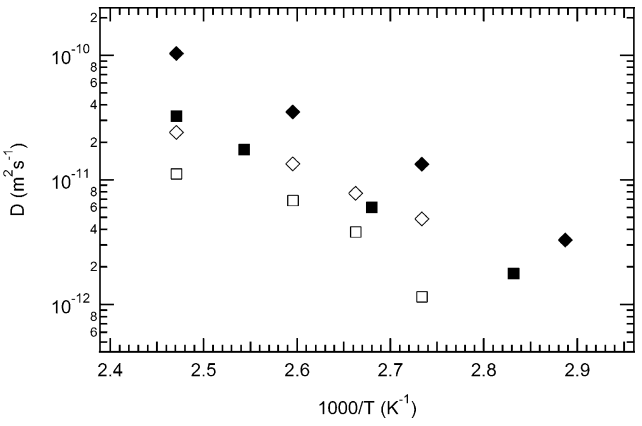


**Figure 2.** $D_{C-H}$ (diamonds) and $D_{TFSI}$ (squares) as a function of temperature for *d*P2VP/nonstoichiometric [Im][TFSI] (solid symbols) and *d*PS-*b*-*d*P2VP/nonstoichiometric [Im][TFSI] (open symbols).

Cation diffusion is deduced from $D_{C-H}$, which is actually a molar-weighted average of the diffusion coefficients of imidazolium cations and neutral imidazole.[28] It is possible, then, that an increase in ion aggregation upon mixing the ionic liquid with the lower dielectric polymer could lead to a larger decrease in $D_{TFSI}$ than $D_{C-H}$ and explain the results in Figure 2. $D_{TFSI,St}$ and $D_{C-H,St}$ were also measured for mixtures of stoichiometric [Im][TFSI] with *d*P2VP and *d*PS-*b*-*d*P2VP, in which the ratio of Im/*d*2VP was held constant to that in the nonstoichiometric mixtures. When a stoichiometric ionic liquid is used, diffusion is dominated by the diffusion of ions. At high temperatures, the difference in the diffusion rate of the anion and cation is similar to that in the nonstoichiometric mixtures (Figure S4 in the Supporting Information), confirming that the high cation diffusion in the nonstoichiometric mixtures is real and not due to fast diffusion of neutral imidazole.

The discrepancy between anion and cation diffusion is smaller in the block copolymer mixture than in the homopolymer mixture. For instance, at 132 °C, $D_{C-H}/D_{TFSI}$ = 3.2 for the homopolymer mixed with ionic liquid compared with $D_{C-H}/D_{TFSI}$ = 2.3 for the analogous block copolymer mixture. This is not surprising given that in the block copolymer portions of the *d*P2VP block close to the block copolymer interface are highly stretched, which appears to affect ion coordination.[19] Similarly, coordination of P2VP with metal chlorides has also been shown to be intimately related to chain conformation.[40] Both $D_{C-H}$ and $D_{TFSI}$ are smaller in the block copolymer mixture than in the homopolymer mixture due to the confinement of the ionic liquid diffusion path to interconnected, isotropically oriented lamellar domains with long-range order defects on the length scale of the NMR experiments, including point defects and grain boundaries.[41]

The most striking difference between the mechanism of proton conductivity in mixtures of nonstoichiometric [Im][TFSI] with homopolymer and block copolymer is the greatly increased amount of proton hopping that occurs in the block copolymer sample. The amount of proton hopping was probed by measuring the ratio of the diffusion coefficient of the acidic ionic liquid proton, $D_{H^+}$, to cation diffusion ($D_{C-H}$), where $D_{H^+}$ was calculated by assuming $D_{N-H}$ is a molar weighted average of the diffusion of protons bound to nitrogen atoms on charged imidazolium and neutral imidazole

$$D_{N-H} = xD_{H^+} + (1 - x)D_{C-H} \quad (2)$$

where $x$ is the mole fraction of imidazolium.[28] As shown in Figure 3, the fact that the proton diffusion coefficient is much larger than $D_{C-H}$ suggests there is a significant amount of proton hopping in the neat nonstoichiometric ionic liquid over the entire experimental temperature range (25 to 120 °C). The amount of proton hopping decreases with increasing temperature. This decrease may be related to a number of mechanisms, including increased hydrogen bond length or shortened average lifetime or decreased number of imidazole hydrogen bonds accompanying an increase in temperature.[42,43]

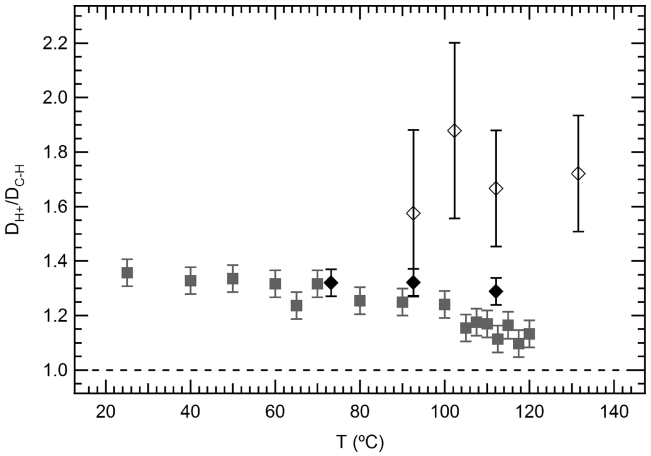


**Figure 3.** Ratio of acidic proton diffusion to cation diffusion as a function of temperature for *d*P2VP/nonstoichiometric [Im][TFSI] (solid diamonds), *d*PS-*b*-*d*P2VP/nonstoichiometric [Im][TFSI] (open diamonds), and neat nonstoichiometric [Im][TFSI] (gray squares). The degree of proton hopping is greatly enhanced in the nanostructured sample. Error bars on data for the neat ionic liquid and the *d*P2VP mixture represent a reasonable estimate based on the reproducibility of experiments, and error bars on data for the *d*PS-*b*-*d*P2VP mixture represent one standard deviation of the mean obtained from many experiments.

Mixing the ionic liquid with *d*P2VP homopolymer does not appear to affect proton-hopping mechanisms. However, the ratio of $D_{H^+}/D_{C-H}$ is considerably greater for the block copolymer mixture, suggesting the influence of confinement on the mechanism of proton transport. Despite the larger error bars for the block copolymer sample (which reflect a decrease in signal following the decrease in proton concentration in these samples), the significant enhancement of acidic proton diffusion is clear.

Further evidence of increased proton hopping in the block copolymer sample comes from QENS experiments. QENS is an ideal tool for studying proton-transport mechanisms because the relatively large incoherent neutron scattering cross section of $^1$H compared with that of other atoms leads to the selective observation of self-correlated hydrogen motion (i.e., diffusion). Motion is probed on the length scale of tenths of nanometers to nanometers, so the local information derived from these experiments compliments NMR diffusion measurements, which are on the micrometer length scale, and bulk ionic conductivity measurements, which are on the millimeter length scale. Representative QENS scattering profiles for mixtures of nonstoichiometric [*d*Im][TFSI] with *d*P2VP homopolymer and *d*PS-*b*-*d*P2VP block copolymer are shown in Figure 4. As the scattering vector $q$ increases, the elastic scattering contribution decreases and the fwhm of the quasi-elastic scattering contribution increases, indicating diffusive motion.[44] This is clearly seen in Figure 4a for the homopolymer sample. The trends are less obvious for the block copolymer sample scattering profiles (Figure 4b) due to a combination of increased $q$-dependent elastic scattering resulting from increased order as well as increased influence of $q$-dependent coherent scattering resulting from a higher concentration of deuterium atoms.[44] The quasi-elastic contributions were modeled to quantify their dependence on $q$. Example fits of

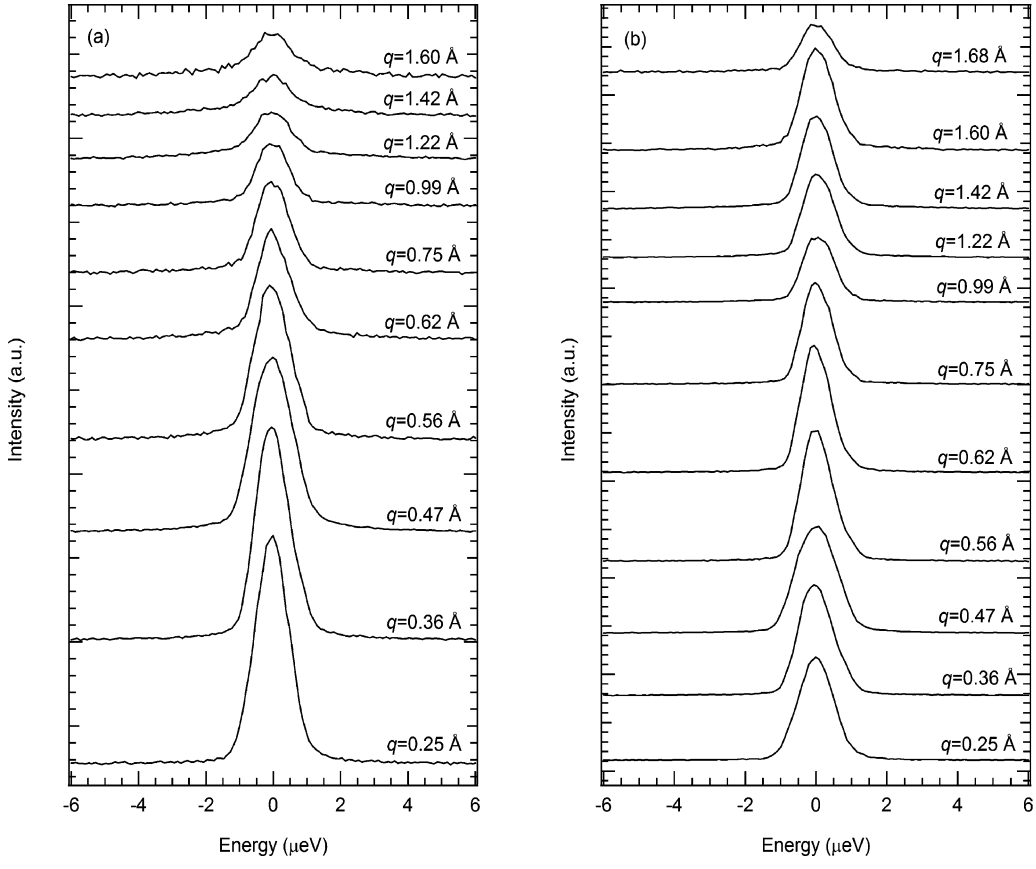


**Figure 4.** QENS scattering profiles of (a) *d*P2VP/nonstoichiometric [*d*Im][TFSI] and (b) *d*PS-*b*-*d*P2VP/nonstoichiometric [*d*Im][TFSI] at 140 °C.

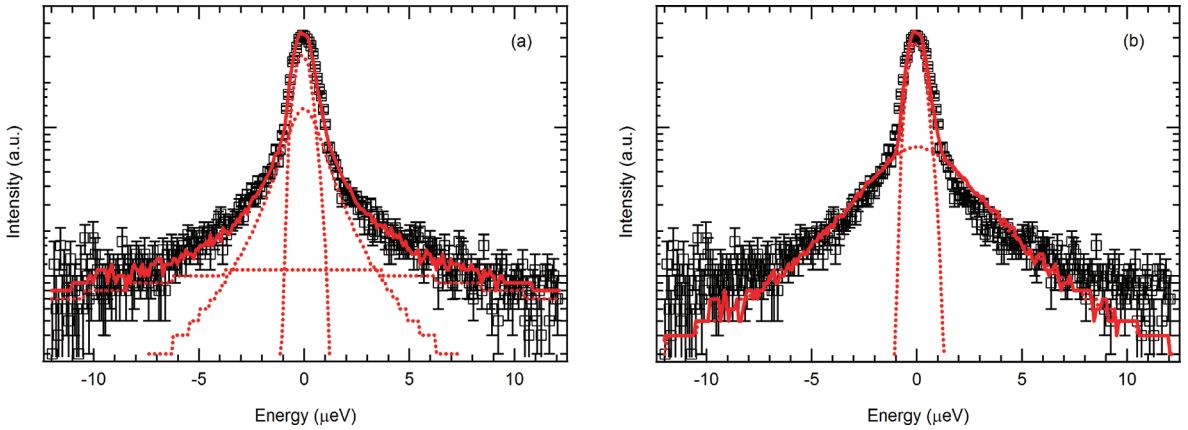


**Figure 5.** QENS profiles of *d*P2VP/nonstoichiometric [*d*Im][TFSI] at $T$ = 140 °C and $q$ = 0.99 Å$^{-1}$. The solid lines are the total fits to the data, whereas the dotted lines are the component fits. The fit using two Lorentzians in addition to a delta function convoluted with the resolution function that captures elastic scattering (a) is clearly better than the fit using a single Lorentzian (b).

the homopolymer sample are shown in Figure 5, where it is clear that two Lorentzian functions are necessary to capture fully the scattering profile: one to describe the main quasi-elastic scattering contribution stemming from diffusive motion and one to describe the high-energy background signal. Similar plots of data and fits for the block copolymer sample are shown in Figure S5 in the Supporting Information.

The $q$ dependence of the fwhm of the main quasi-elastic scattering contribution, Γ, provides information regarding the mechanism of proton diffusion. When there is purely Fickian diffusion, Γ is expected to vary linearly with $q^2$ according to[44]

$$\Gamma/2 = \hbar D q^2 \tag{3}$$

Equation 3 adequately describes simple liquids such as argon[45] and even some more complex liquids such as the ionic liquid 1-butyl-3-methylimidazolium:chloride.[46] When molecular interactions are significant, for instance, in the case of the ionic liquids 1-ethyl-3-methylimidazolium:bromide[47] and *N*,*N*,*N*′,*N*′-tetramethylguanidinium:bis(perfluoroethylsulfonyl)imide,[48] deviations from eq 3 have been observed at high values of $q$ corresponding to length scales smaller than the interaction distance. In these cases, the jump-diffusion model[49] has been used to describe the variation of Γ with $q^2$ as

$$\Gamma/2 = \frac{\hbar D q^2}{1 + D q^2 \tau_0} \tag{4}$$

where $\tau_0$ is the residence time between jumps or the molecular interaction time. Specifically, the jump-diffusion model describes the complex dynamics of protons in supercooled water, which are dominated by Grotthuss proton transfer between water molecules through hydrogen bonds.[50,51] $\tau_0$ in this case is the time between proton-transfer events. Similarly, eq 4 is a good model for describing quasi-elastic scattering from the combination of diffusion and proton hopping in non-stoichiometric [*d*Im][TFSI], where the interpretation of $\tau_0$ is complex because of significant contributions of both molecular interactions and proton hopping to the deviation from Fickian behavior.[39] Therefore, it is expected that the ionic liquid/polymer mixtures in this study also exhibit non-Fickian behavior that can be estimated by eq 4 and that the magnitude of the departure from Fickian behavior is related to the amount of proton hopping. Figure 6 demonstrates that the acidic protons in mixtures of nonstoichiometric [*d*Im][TFSI] with

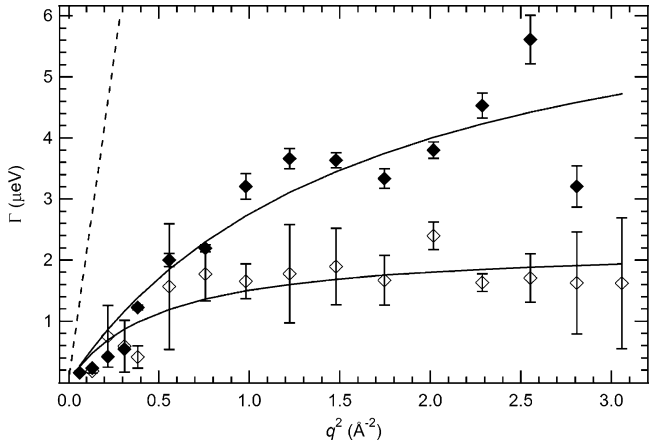


**Figure 6.** Γ of the main Lorentzian peak fit to QENS scattering profiles as a function of $q^2$ for *d*P2VP/nonstoichiometric [*d*Im][TFSI] (solid symbols) and *d*PS-*b*-*d*P2VP/nonstoichiometric [*d*Im][TFSI] (open symbols) at 140 °C. Error bars represent one standard deviation of the fits. Solid curves are fits to the data using eq 4, and the dashed line is the Fickian diffusion curve (eq 3) using $D_{N-H}$ in the homopolymer sample from NMR.

*d*P2VP homopolymer and *d*PS-*b*-*d*P2VP block copolymer undergo non-Fickian diffusion, adequately captured by eq 4. The block copolymer sample shows a greater departure from Fickian diffusion than the homopolymer sample, indicating increased proton hopping in agreement with NMR diffusion experiments.

It is anticipated that increased proton hopping in the block copolymer sample is related to a difference in the imidazole hydrogen bond structure under confinement. The $^1$H MAS NMR chemical shifts of the protons covalently bound to imidazole/imidazolium nitrogens, $\delta_{N-H}$, are strongly dependent on hydrogen bonding.[28] In qualitative similarity with the neat ionic liquid,[39] $\delta_{N-H}$ shifts to lower ppm as the temperature is increased (Figure 7a,7b). The temperature dependence of $\delta_{N-H}$ is steeper for the block copolymer mixture than for the neat ionic liquid sample and the homopolymer mixture (Figure 7c), suggesting unique hydrogen-bonding behavior. Furthermore, the absolute values of the chemical shifts for the block copolymer sample are unexpected. The higher values for the homopolymer sample compared with those for the neat ionic liquid are unsurprising due to the greater number of molecules


dx.doi.org/10.1021/ma202741g | *Macromolecules* 2012, 45, 3112–3120

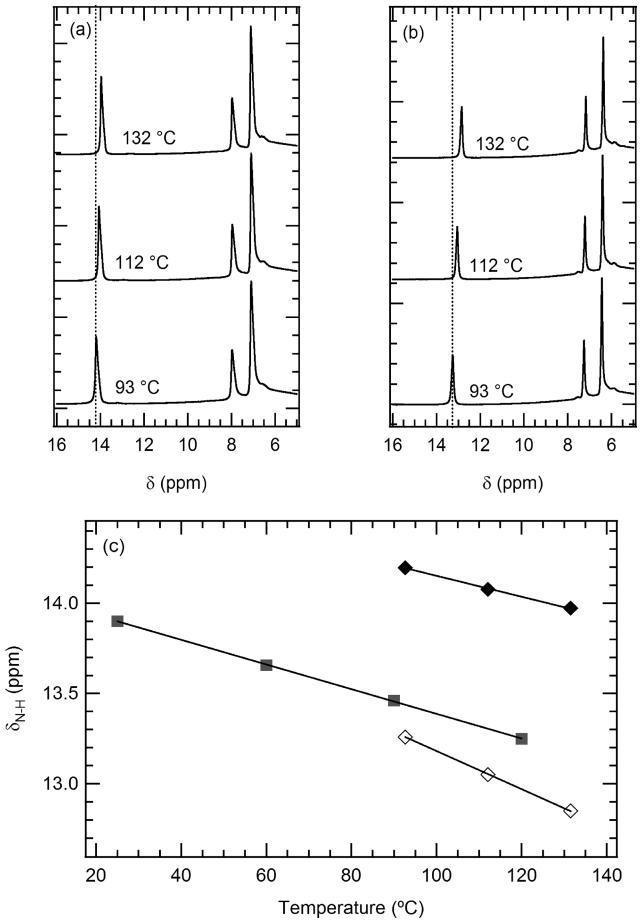


**Figure 7.** MAS $^1$H NMR spectra of (a) *d*P2VP/nonstoichiometric [Im][TFSI] and (b) *d*PS-*b*-*d*P2VP/nonstoichiometric [Im][TFSI] as well as (c) $\delta_{N-H}$ as a function of temperature for the *d*P2VP mixture (solid diamonds), *d*PS-*b*-*d*P2VP mixture (open diamonds), and neat nonstoichiometric [Im][TFSI] (gray squares). Lines of best linear fit connect the data points.

that can participate in hydrogen bonding. The same phenomena is observed when excess imidazole is added to stoichiometric ionic liquid.[28] The block copolymer sample has lower values of $\delta_{N-H}$ despite containing the same number of molecules that can participate in hydrogen bonding as the homopolymer sample. These unexpected trends indicate that a different hydrogen bond network exists in the ionic liquid when confined to block copolymer domains, which affects the amount of proton hopping that occurs.

Polymer chain stretching near the block copolymer interface likely affects how *d*2VP units interact with the imidazole hydrogen bond network. Previous studies have already demonstrated the relationship between polymer chain conformation and ion and metal chloride coordination.[19,40] Additionally, the presence of the interface itself likely alters the near-interface hydrogen bond structure, the effects of which could propagate several nanometers into either side of the 17 nm *d*P2VP/ionic liquid channels. Such confinement effects on hydrogen bonding in water are well-documented.[10−13]

The mechanistic differences in proton transport in the nanostructured and nonordered samples lead to differences in bulk ionic conductivity, $\sigma$. In Figure 8, $\sigma$ is plotted as a function of temperature for mixtures of nonstoichiometric [Im][TFSI] with homopolymer and block copolymer. The conductivity of

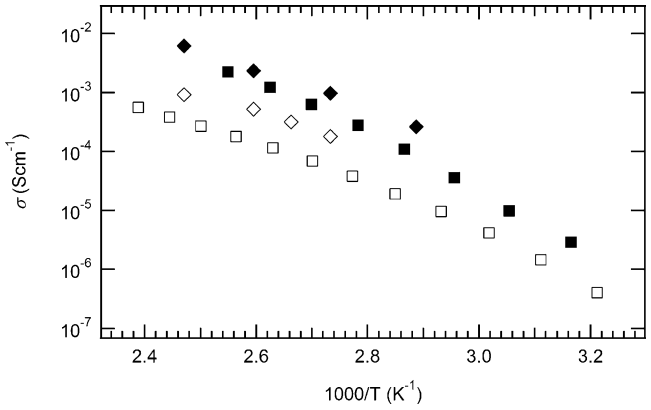


**Figure 8.** Measured $\sigma$ (squares) and $\sigma$ calculated from NMR diffusion coefficients and the Nernst−Einstein equation (diamonds) for mixtures of nonstoichiometric [Im][TFSI] with P2VP (solid symbols) and PS-*b*-P2VP (open symbols).

the block copolymer sample is lower than that of the homopolymer sample due to the overall lower ion concentration in the block copolymer membrane, in addition to the lack of long-range order characterizing its lamellar domains. Ion aggregation in each sample is investigated by comparing the measured conductivity to the conductivity predicted by the Nernst−Einstein equation using ion diffusion coefficients measured by NMR. The Nernst−Einstein equation is given by

$$\sigma = \frac{F^2}{RT}(c_{m,H^+}D_{H^+} + c_{m,TFSI}D_{TFSI}) \quad (5)$$

where $c_{m,H^+}$ and $c_{m,TFSI}$ are the molar concentrations of acidic protons and TFSI anions, respectively. The predicted conductivities for both samples are plotted along with the measured bulk conductivities as a function of temperature in Figure 8. Equation 5 overpredicts the measured ionic conductivity of the block copolymer sample by a factor of 3 to 4 while predicting the homopolymer conductivity relatively well. Because NMR measures diffusion over micrometer length scales and bulk conductivity measurements probe a millimeter dimension, the large discrepancy for the block copolymer sample is likely attributed to a combination of ion aggregation and differences in long-range order. The increasing overprediction of the conductivity of the homopolymer sample at lower temperatures suggests an increase in the degree of ion aggregation with decreasing temperature. The strong temperature dependence suggests that anionic aggregates are not the major cause of faster relative cation diffusion in the homopolymer sample. (If the ion aggregates were anionic aggregates, the temperature dependence would be reflected in Figure 2.) In the block copolymer sample, no temperature dependence is observed, so anionic aggregates in this sample are still a possibility.

The result of different ion aggregation behavior as well as different amounts of proton hopping in the homopolymer and block copolymer samples is that the activation energy for bulk ionic conductivity is lower in the block copolymer sample. This is clearly observed in Figure 8, where the temperature dependence for the measured conductivity is much less steep.

## ■ CONCLUSIONS

Proton transport in ionic liquids is clearly affected when the ionic liquid is mixed with a polymer and especially when the


dx.doi.org/10.1021/ma202741g | *Macromolecules* 2012, 45, 3112−3120

ionic liquid is confined to block copolymer nanodomains. Several specific mechanistic changes have been illuminated in this work using a combination of transport measurements that together probe a variety of length scales and a variety of molecular and atomic species. The relative amount of cation and anion diffusion, for example, has been found to change drastically upon incorporation of ionic liquid into a homopolymer and block copolymer. In the case presented here of nonstoichiometric [Im][TFSI] mixed with *d*P2VP and *d*PS-*b*-*d*P2VP, specific interactions between TFSI and *d*2VP moieties or the prevalence of anionic aggregates cause the cation to diffuse significantly faster than the anion, which is in stark contrast with the neat ionic liquid. This asymmetric charge transport could be taken advantage of for a variety of applications, including proton exchange membrane fuel cells or actuators.

The temperature dependence of ion aggregation has been found to be significantly different in the homopolymer and block copolymer samples, contributing to a lower activation energy for ion transport in the block copolymer sample. Determining the degree of ion aggregation in the block copolymer sample as well as understanding the source of its temperature independence could lead to the design of nanostructured membranes with increased conductivity.

The most striking change in proton transport upon incorporation of nonstoichiometric [Im][TFSI] into a block copolymer is that the amount of diffusion-enhancing proton-hopping drastically increases. We propose that block copolymer chain stretching or confinement affect the hydrogen-bond structure of the ionic liquid, leading to this increase. Long-range proton diffusion in the block copolymer/ionic liquid membrane is still not as high as in the homopolymer/ionic liquid membrane because of the lack of long-range order characterizing the lamellar domains. However, highly conductive, mechanically durable membranes could be designed by combining the enhancement of acidic proton diffusion due to block copolymer self-assembly with increased long-range order obtained using one of many channel-aligning techniques.[52]

## ■ ASSOCIATED CONTENT

### Supporting Information

SAXS morphological characterization of block copolymer/ionic liquid mixtures, representative PGSE NMR data, diffusion data as a function of experimental diffusion time, representative QENS fits, and diffusion data for control mixtures of polymer with stoichiometric [Im][TFSI]. This material is available free of charge via the Internet at http://pubs.acs.org.

## ■ AUTHOR INFORMATION

### Corresponding Author

*E-mail: mhoarfrost@berkeley.edu.

### Notes

The authors declare no competing financial interest.

## ■ ACKNOWLEDGMENTS

We gratefully acknowledge support from the Assistant Secretary for Energy Efficiency and Renewable Energy, Office of Hydrogen, Fuel Cell, and Infrastructure Technologies of the U.S. Department of Energy under contract DE-AC02-05CH11231. M.L.H. acknowledges support from an NSF Graduate Research Fellowship. SAXS experiments were performed at the ALS and the SSRL. Both are national user facilities supported by the Department of Energy, Office of Basic Sciences. We gratefully acknowledge Dr. Alexander Hexemer, Dr. Cheng Wang, and Dr. Eric Schaible for experimental assistance at the ALS and Dr. John Pople for experimental assistance at the SSRL. This work also utilized facilities at the NCNR partially supported by the National Science Foundation under agreement no. DMR-0944772. We gratefully acknowledge Dr. Timothy Jenkins for experimental assistance at the NCNR. Finally, we thank Dr. Joel Stettler for technical assistance with NMR experiments. Certain commercial equipment, instruments, materials or material suppliers are identified in this Article to foster understanding. Such identification does not imply recommendation or endorsement by the National Institute of Standards and Technology, nor does it imply that the materials or equipment identified are necessarily the best available for the purpose.

## ■ REFERENCES

(1) Mauritz, K. A.; Moore, R. B. *Chem. Rev.* **2004**, *104* (10), 4535−4585.
(2) Chen, Y. B.; Thorn, M.; Christensen, S.; Versek, C.; Poe, A.; Hayward, R. C.; Tuominen, M. T.; Thayumanavan, S. *Nat. Chem.* **2010**, *2* (6), 503−508.
(3) Ichikawa, T.; Yoshio, M.; Hamasaki, A.; Mukai, T.; Ohno, H.; Kato, T. *J. Am. Chem. Soc.* **2007**, *129* (35), 10662−10663.
(4) Wanakule, N. S.; Panday, A.; Mullin, S. A.; Gann, E.; Hexemer, A.; Balsara, N. P. *Macromolecules* **2009**, *42* (15), 5642−5651.
(5) Rubatat, L.; Li, C. X.; Dietsch, H.; Nykanen, A.; Ruokolainen, J.; Mezzenga, R. *Macromolecules* **2008**, *41* (21), 8130−8137.
(6) Ruzette, A. V. G.; Soo, P. P.; Sadoway, D. R.; Mayes, A. M. *J. Electrochem. Soc.* **2001**, *148* (6), A537−A543.
(7) Hoarfrost, M. L.; Segalman, R. A. *Macromolecules* **2011**, *44* (13), 5281−5288.
(8) Cho, B. K.; Jain, A.; Gruner, S. M.; Wiesner, U. *Science* **2004**, *305* (5690), 1598−1601.
(9) Kim, Y. S.; Pivovar, B. S. *Annu. Rev. Chem. Biomol. Eng.* **2010**, *1*, 123−148.
(10) Scatena, L. F.; Brown, M. G.; Richmond, G. L. *Science* **2001**, *292* (5518), 908−912.
(11) Piletic, I. R.; Moilanen, D. E.; Spry, D. B.; Levinger, N. E.; Fayer, M. D. *J. Phys. Chem. A* **2006**, *110* (34), 10369−10369.
(12) Moilanen, D. E.; Levinger, N. E.; Spry, D. B.; Fayer, M. D. *J. Am. Chem. Soc.* **2007**, *129* (46), 14311−14318.
(13) Guegan, R. *J. Colloid Interface Sci.* **2011**, *358* (2), 485−490.
(14) Moilanen, D. E.; Piletic, I. R.; Fayer, M. D. *J. Phys. Chem. C* **2007**, *111* (25), 8884−8891.
(15) Choi, P.; Jalani, N. H.; Datta, R. *J. Electrochem. Soc.* **2005**, *152* (3), E123−E130.
(16) Eikerling, M.; Kornyshev, A. A.; Kuznetsov, A. M.; Ulstrup, J.; Walbran, S. *J. Phys. Chem. B* **2001**, *105* (17), 3646−3662.
(17) Mafe, S.; Manzanares, J. A.; Ramirez, P. *Phys. Chem. Chem. Phys.* **2003**, *5* (2), 376−383.
(18) Paddison, S. J.; Paul, R. *Phys. Chem. Chem. Phys.* **2002**, *4* (7), 1158−1163.
(19) Singh, M.; Odusanya, O.; Wilmes, G. M.; Eitouni, H. B.; Gomez, E. D.; Patel, A. J.; Chen, V. L.; Park, M. J.; Fragouli, P.; Iatrou, H.; Hadjichristidis, N.; Cookson, D.; Balsara, N. P. *Macromolecules* **2007**, *40* (13), 4578−4585.
(20) Bureekaew, S.; Horike, S.; Higuchi, M.; Mizuno, M.; Kawamura, T.; Tanaka, D.; Yanai, N.; Kitagawa, S. *Nat. Mater.* **2009**, *8* (10), 831−836.
(21) Simone, P. M.; Lodge, T. P. *ACS Appl. Mater. Interfaces* **2009**, *1* (12), 2812−2820.
(22) Simone, P. M.; Lodge, T. P. *Macromolecules* **2008**, *41* (5), 1753−1759.
(23) Virgili, J. M.; Hexemer, A.; Pople, J. A.; Segalman, R. A.; Balsara, N. P. *Macromolecules* **2009**, *42* (13), 4604−4613.

(24) Virgili, J. M.; Nedoma, A. J.; Segalman, R. A.; Balsara, N. P. *Macromolecules* **2010**, *43* (8), 3750−3756.
(25) Virgili, J. M.; Hoarfrost, M. L.; Segalman, R. A. *Macromolecules* **2010**, *43* (12), 5417−5423.
(26) Gwee, L.; Choi, J. H.; Winey, K. I.; Elabd, Y. A. *Polymer* **2010**, *51* (23), 5516−5524.
(27) Munch, W.; Kreuer, K. D.; Silvestri, W.; Maier, J.; Seifert, G. *Solid State Ionics* **2001**, *145* (1−4), 437−443.
(28) Noda, A.; Susan, A. B.; Kudo, K.; Mitsushima, S.; Hayamizu, K.; Watanabe, M. *J. Phys. Chem. B* **2003**, *107* (17), 4024−4033.
(29) Kreuer, K. D.; Fuchs, A.; Ise, M.; Spaeth, M.; Maier, J. *Electrochim. Acta* **1998**, *43* (10−11), 1281−1288.
(30) Kim, S. Y.; Kim, S.; Park, M. J. *Nat. Commun.* **2010**, *1*, 88.
(31) Kim, S. Y.; Yoon, E.; Joo, T.; Park, M. J. *Macromolecules* **2011**, *44* (13), 5289−5298.
(32) Hou, J. B.; Zhang, Z. Y.; Madsen, L. A. *J. Phys. Chem. B* **2011**, *115* (16), 4576−4582.
(33) Susan, M. A.; Kaneko, T.; Noda, A.; Watanabe, M. *J. Am. Chem. Soc.* **2005**, *127* (13), 4976−4983.
(34) Yokoyama, H.; Mates, T. E.; Kramer, E. J. *Macromolecules* **2000**, *33* (5), 1888−1898.
(35) Price, W. S. *Concepts Magn. Reson.* **1998**, *10* (4), 197−237.
(36) Stejskal, E. O.; Tanner, J. E. *J. Chem. Phys.* **1965**, *42* (1), 288−292.
(37) Raiford, D. S.; Fisk, C. L.; Becker, E. D. *Anal. Chem.* **1979**, *51* (12), 2050−2051.
(38) Azuah, R. T.; Kneller, L. R.; Qiu, Y. M.; Tregenna-Piggott, P. L. W.; Brown, C. M.; Copley, J. R. D.; Dimeo, R. M. *J. Res. Natl. Inst. Stand. Technol.* **2009**, *114* (6), 341−358.
(39) Hoarfrost, M. L.; Tyagi, M. S.; Segalman, R. A.; Reimer, J. A., in preparation.
(40) Lee, D. H.; Kim, H. Y.; Kim, J. K.; Huh, J.; Ryu, D. Y. *Macromolecules* **2006**, *39* (6), 2027−2030.
(41) Hou, J. B.; Li, J.; Madsen, L. A. *Macromolecules* **2010**, *43* (1), 347−353.
(42) Kanaskov, Yd; Sukhoruk, Bi; Pentin, Y. A.; Komarovs, Gv. *Izv. Akad. Nauk SSSR, Ser. Khim.* **1970**, *8*, 1735.
(43) Cavalcanti, W. L.; Portaluppi, D. F.; Joswig, J. O. *J. Chem. Phys.* **2010**, *133* (10), 104703.
(44) Bée, M. *Quasielastic Neutron Scattering: Principles and Applications in Solid State Chemistry, Biology and Materials Science* IOP Publishing Ltd: Bristol, U.K., 1988.
(45) Dasannacharya, B. A.; Rao, K. R. *Phys. Rev.* **1965**, *137* (2A), A417−A427.
(46) Inamura, Y.; Yamamuro, O.; Hayashi, S.; Hamaguchi, H. O. *Phys. B* **2006**, *385*, 732−734.
(47) Aoun, B.; Gonzalez, M. A.; Ollivier, J.; Russina, M.; Izaola, Z.; Price, D. L.; Saboungi, M. L. *J. Phys. Chem. Lett.* **2010**, *1* (17), 2503−2507.
(48) Mamontov, E.; Luo, H. M.; Dai, S. *J. Phys. Chem. B* **2009**, *113* (1), 159−169.
(49) Chudley, C. T.; Elliott, R. J. *Proc. Phys. Soc., London* **1961**, *77* (494), 353−361.
(50) Chen, S. H.; Teixeira, J.; Nicklow, R. *Phys. Rev. A* **1982**, *26* (6), 3477−3482.
(51) Teixeira, J.; Bellissentfunel, M. C.; Chen, S. H.; Dianoux, A. J. *Phys. Rev. A* **1985**, *31* (3), 1913−1917.
(52) Li, J.; Park, J. K.; Moore, R. B.; Madsen, L. A. *Nat. Mater.* **2011**, *10* (7), 507−511.